Mar. Sci. Tech. Bull. (2022) 11(1): 41-51
e–ISSN: 2147–9666
info@masteb.com

dergipark.org.tr/en/pub/masteb
www.masteb.com
DOI: 10.33714/masteb.1066936

Marine Science and Technology Bulletin

RESEARCH ARTICLE

On the hydrodynamic effects of the eidonomy of the hammerhead shark's cephalofoil in the eye bulb region: Winglet-like behaviour

Arash Taheri[1*]

[1] *Division of Applied Computational Fluid Dynamics, Biomimetic and Bionic Design Group, 13439, Tehran, Iran*

ARTICLE INFO

Article History:
Received: 02.02.2022
Received in revised form: 03.03.2022
Accepted: 03.03.2022
Available online: 21.03.2022

Keywords:
Cephalofoil
Hammerhead sharks
Bionic winglet
CFD
Functional eidonomy
Ichthyology

ABSTRACT

External morphology (eidonomy) of marine creatures, developed by the evolution process over the course of millions of years, plays a crucial role in their locomotion and swimming performance. In this paper, hydrodynamic impacts of the cephalofoil tip eidonomy (tip bump) in the eye bulb region of a scalloped hammerhead shark, *Sphyrna lewini*, are studied with the aid of computational fluid dynamics (CFD). In this regard, two separate geometries are designed here; one corresponding to the real geometry of the hammerhead shark's cephalofoil with a tip bump (eye bulb region) and another one, a modified version with a flat tip without the aforementioned bump. Turbulent flows encountered in the problem are simulated using the Lam-Bremhorst turbulence model at different angles of attack (AoA) and a sideslip angle, at high Reynolds number, 10^6, corresponding to the swimming of a juvenile hammerhead shark with a speed of 1 m/s. The results show that the strength (circulation) of the wing tip vortices reduces by the external geometry of the hammerhead's cephalofoil tip; in this sense, 'cephalofoil tip' with its unique morphology behaves as a winglet.

Please cite this paper as follows:

Taheri, A. (2022). On the hydrodynamic effects of the eidonomy of the hammerhead shark's cephalofoil in the eye bulb region: Winglet-like behaviour. *Marine Science and Technology Bulletin*, *11*(1), 41-51. https://doi.org/10.33714/masteb.1066936

Introduction

In general, two major factors determine the swimming performance and locomotion of swimming animals, including: animal's body deflection as a function of time (i.e., deflection dynamics) and animal's external morphology or eidonomy (Taheri, 2021a). Many marine faunas such as fishes (including sharks and rays), cetaceans (whales and dolphins), and jellyfish, utilize the concept of repetitive 'body deflection' in vast varieties to propel themselves in the aquatic environment. Computational fluid dynamics (CFD) can be successfully adopted to simulate fluid flow generated in the downstream wake of a swimming animal and also locomotion and propulsion generation by aquatic animals; such as anguilliform and carangiform swimmers (Borazjani, 2008), jellyfish (Taheri, 2018a; Miles and Battista, 2019), swimming nematode (Battista,

* Corresponding author
E-mail address: taha.bionics@gmail.com (A. Taheri)

2020; Taheri, 2021b) and manta rays (Fish et al., 2016), to name a few.

External morphology (eidonomy) of a swimming animal in interaction with its habitat (aquatic environment), as a major factor, determines important fluid flow phenomena encountered in the swimming process, such as: vortical structure generation and merger, flow separation and reattachment, etc. In other words, the presence of some morphological features on the external surface of the animal's body can potentially bring some favourable hydrodynamic effects for locomotion and swimming of the animal. For example, a wavy/undulatory geometric pattern at the leading edge of humpback whale's flippers leads to the formation of streamwise vortices; this leads to a stall delay and can typically provide better hydrodynamic performance at post-stall region (Miklosovic, 2004; Taheri, 2018b). As other instances of hydrodynamic effects of the external morphology, one can consider effects of ventral pleats on the belly of humpback whales (Taheri, 2018c), denticles on the sharkskin (Domel et al., 2018), ridges on the carapace of leatherback turtles (Bang et al., 2016) and longitudinal ridges on the dorsal area of whale sharks (Taheri, 2020). As an example of adverse (unfavourable) hydrodynamic effects of the external morphology on the locomotion, one can look at the effects of manta ray injuries (geometric deficiencies), generated by predator's attacks or boat strikes, on the manta ray gliding performance (Taheri, 2021c). In the present paper, external geometry of the scalloped hammerhead shark's cephalofoil is examined for possible favourable hydrodynamic characteristics.

Hammerhead sharks, *Sphyrnidae* family, are among charismatic aquatic animals in ocean and sea inshore. In this family, *Sphyrna lewini* as a scalloped hammerhead shark is a seasonally migratory shark and can be found worldwide in warm/tropical sea/ocean waters, such as the 'Persian Gulf' in the south of Iran. Their maximum total body length can reach 3.7-4.2 m at maturity (Copmpagno et al., 2005). In general, hammerhead shark is among agile swimmers in its habitat including ocean and sea inshore from the surface to deep waters (deeper than 275 m). Their swimming speed is about 1 m/s at cruise and can reach about 10 m/s at burst swimming (Ketchum et al., 2014). These species can be simply identified by the special shape of their head, i.e., cephalofoil, resembling a hammer-shape (Figure 1). The abovementioned unique morphology provides a higher level of stereoscopic vision (Copmpagno et al., 2005; McComb et al., 2009; Kuznar, 2017), olfactory (Kajiura et al., 2005; Kuznar, 2017) and electro-sensory capabilities (Kuznar, 2017) for the aquatic animal. Researchers have also studied the functionality of cephalofoil in the enhanced manoeuvrability of hammerhead sharks (Kajiura et al., 2003; Gaylord et al., 2020).

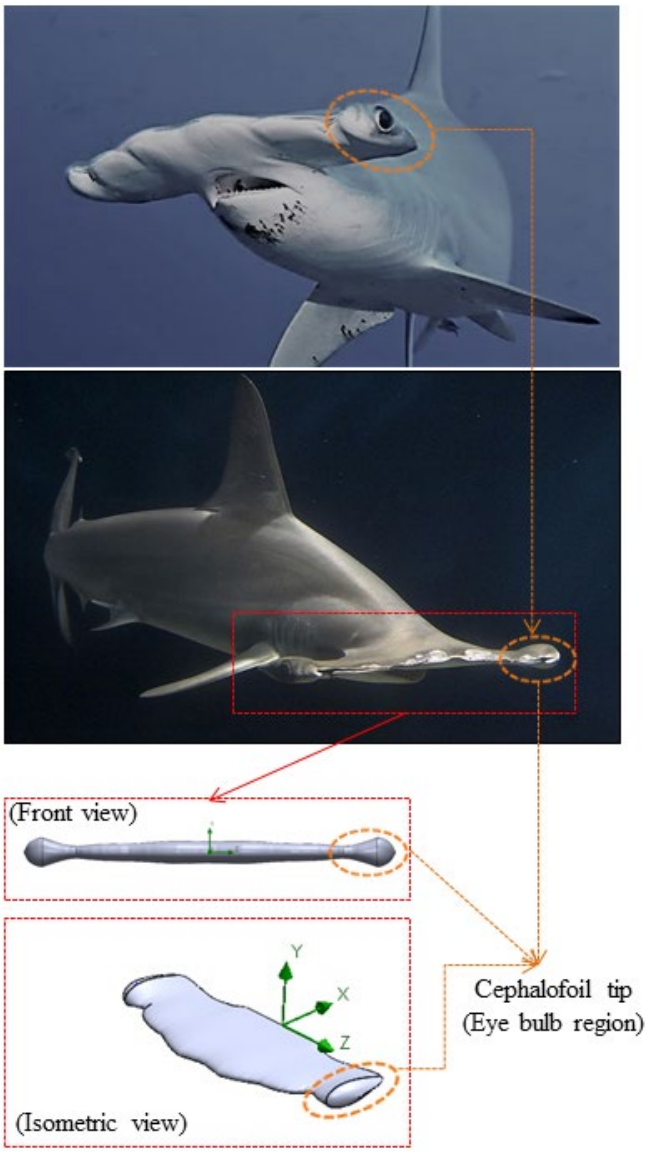

Figure 1. Geometry of the cephalofoil tip (eye bulb region) of a scalloped hammerhead shark, *S. lewini* [real geometry: top (source: twofishdivers) & middle (source: Suneko, Flickr); bottom: 3D modelled geometry]

In the present study, the evolution and characteristics of the 'tip vortex' induced by the special morphology of the cephalofoil tip of a scalloped hammerhead shark are studied (Figure 1). Our results indicate a 'winglet-like' behaviour for the cephalofoil tip of the hammerhead shark.

Materials and Methods

Computational fluid dynamics (CFD) is adopted here to study flow passing around the cephalofoil of a scalloped hammerhead shark, *S. lewini*. In general, numerical flow

simulations can provide a comprehensive and more complete data set to investigate details of the flow field without limitations of the experimental techniques. In principle, CFD simulations can behave as a platform or numerical 'test rig' to study fluid flow phenomena in details and from different angles, which can be extremely helpful to grasp underlying mechanisms involved in the physics of the problem. Here, the comparative CFD simulation technique, as a powerful method in the field of bionic designs and Biomimetics, is utilized to explore the effects of the external morphology of the cephalofoil tip on the 'tip vortex' characteristics.

Geometry Models of Hammerhead Shark's Cephalofoil

Two geometries are designed to observe the hydrodynamic effects of the cephalofoil tip. The first model resembles the real geometry of the hammerhead shark's cephalofoil with tip bump, basically generated by the presence of the eye bulb (Figure 2, part A). Another geometric model is a modified version, identical to the first model except for the tip region, which is flat here without the abovementioned bump (Figure 2, part B). To construct a 3D model of the cephalofoil (Figure 2, part A), hydrofoil ribs of a scaled-down cephalofoil model are scanned and digitalized in some selected planes perpendicular to the lateral (z) axis. Overall, a total number of 13 cross-sections and 2 guide curves representing L.E. and T.E. of the cephalofoil (in the plane defined as y=0) are generated in MATLAB with high resolution and imported into the SolidWorks CAD environment. Then, the cephalofoil model is constructed by applying a so-called 'Lofting process'. The aforementioned process is performed by stitching the successive rib-section curves one by one, controlled by 2 guide curves.

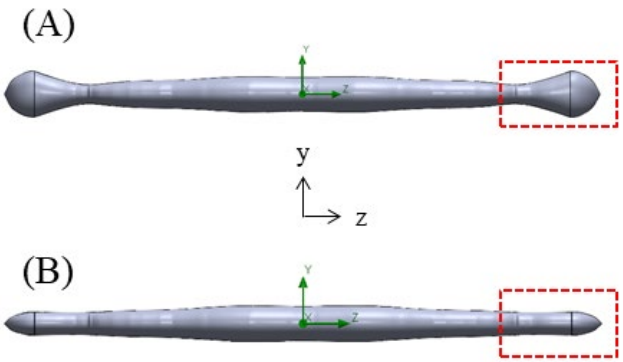

Figure 2. Adopted 3D cephalofoil geometry for a scalloped hammerhead shark: A) Real cephalofoil- geometry with a tip bump (eye bulb); B) Modified cephalofoil- imaginary geometry with a flat tip, i.e., without the tip bump (eye bulb)

Numerical Methodology

For upcoming simulations, inflow velocity is set based on a prescribed Reynolds number, i.e., 10^6, corresponding to the swimming of a juvenile hammerhead shark at low swimming speed mode with a velocity equal to 1 m/s. Water current in the aquatic environment is another factor that contributes to the calculations. In general, ocean currents vary widely geographically. As an instance, in western North Atlantic Ocean, fastest current speed is about 2.5 m/s near the ocean surface and its gulf current speed is equal to 1.8 m/s. A combination of the swimming speed with ocean and sea currents generates a wide range of angles of attack (AoA) and sideslip angles for the hammerhead shark. It is also worth mentioning that adult scalloped hammerhead sharks spend the majority of their time swimming at a rolled angle (Royer et al., 2020) to reduce transports costs (Payne et al., 2016). Figure 3 shows the coordinate system adopted to define AoA (α) and sideslip angle (ψ) for all upcoming simulations. In this regard, the shark's body and its cephalofoil are placed in a fixed position in space and the aforementioned angles α and ψ are defined by a blowing angle relative to the streamwise (x) direction. In the planned computation campaign here, a total number of 20 simulations at different AoAs and a sideslip angle are performed.

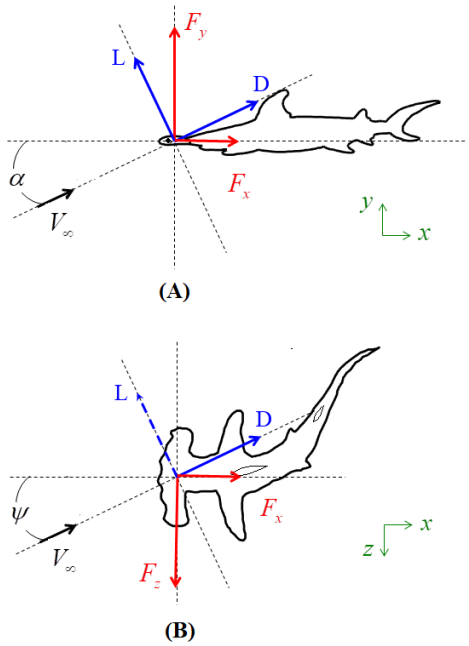

Figure 3. Coordinate system adopted for turbulent flow simulations over the cephalofoil; A) angle of attack (AoA), B) sideslip angle

Computational Domain and Grid Generation

The computational domain is considered as a cube around the cephalofoil. To minimize the boundary effects, it extends 2.5 times of the cephalofoil span (b) in y^- and y^+ vertical directions; 2 and 3 times of cephalofoil span in x^- and x^+ streamwise directions, respectively and 2 times of cephalofoil span in z^- and z^+ lateral directions (Figure 4). A larger extension in x^+ direction allows capturing tip vortices in full size in the computational domain. SolidWorks meshing tool with an adaptive mesh capability is adopted in the present study to construct a computational grid around the cephalofoil. After a mesh convergence test, a well-converged grid with a maximum of 2 million elements is adopted for all upcoming simulations. As one can see in Figure 4, through three levels of mesh refinements a smooth transition between the coarse mesh in the outer-flow region and fine mesh in the near-body zone is obtained. It is visible that the adaptive mesh can properly capture all fine features of the cephalofoil geometry and its corresponding boundary layers.

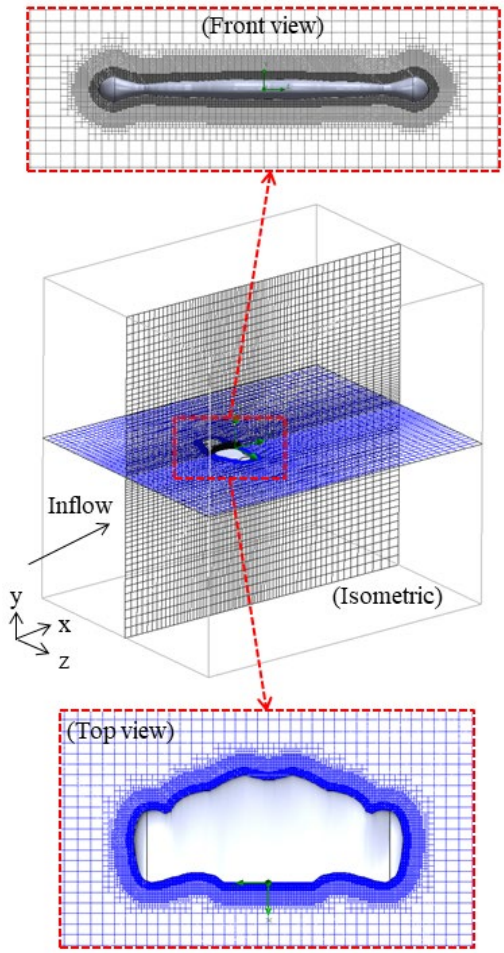

Figure 4. Computational domain with an adaptive grid generation around the cephalofoil geometry of *S. lewini*

Flow Solver & Turbulence Treatment

Incompressible Navier-Stokes equations are the governing equations of turbulent flows passing over the hammerhead shark's cephalofoil. Turbulence at high Reynolds number, $Re \sim 10^6$, is treated here using the Lam-Bremhorst turbulence model (Lam & Bremhorst, 1981) by SolidWorks Flow Simulation (SFS) solver. The solver utilizes the finite volume method along with the URANS-SIMPLE technique to obtain numerical solutions of the flow fields. In this regard, multigrid, conjugate gradient and operator-splitting techniques are also adopted for an efficient computing performance (Sobachkin & Dumnov, 2013).

For upcoming numerical flow simulations, 'inflow' is set as a prescribed inlet velocity with a blowing angle, as already explained (Figure 3). All other boundaries are set as 'outflow' in the solver. For the calculations, inflow turbulence intensity and length scale are set as 0.1% and 8×10^{-4}, respectively. SFS solver applies a rigorous statistical strategy based on a dynamic calculation of dispersion of flow variables like velocity, pressure, etc. to ensure reaching the lowest residual level for the convergence.

Cephalofoil Tip Vortex Strength

A vortex can be viewed as a relatively long-lived structure in a 3D flow field, which involves a centreline (vortex core) and a border. This entity makes the fluid particles rotate around its centreline in a circular/spiral pattern. To quantify the strength of a vortex, one should see how much powerful the vortex is to make the adjacent fluid particles rotate around its centreline. In this regard, the concept of 'circulation' can be adopted as a practical measure to quantify the strength of a vortex. Circulation (Γ) around a closed curve C in the flow field (here around the vortex core) is defined as below:

$$\Gamma = \oint_C \vec{u}.d\vec{x} = \int_A \vec{\omega}.\vec{n}\,dA \qquad (1)$$

In the above equation, $\vec{u}$ and $\vec{\omega}$ denote velocity and vorticity vectors, respectively. In addition, $d\vec{x}$ stands for differential line element vector along the curve C and $\vec{n}$ is the unit vector perpendicular to the cross-sectional area A (surrounded by the closed curve C).

In general, tip vortices are produced by moving a finite wing in a fluid environment, due to spanwise flow motion which rolls up from the bottom of the wing (high pressure region) to the upper surface of the wing (low pressure region) around the wing tip. This lateral fluid flow motion superimposed with the freestream bulk flow produces a spiral vortical structure

originating from the wing tip, namely a 'tip vortex'. The formation of this kind of vortices leads to an energy loss for the wing flow system, and ultimately increases the 'induced drag' of the wing. Wingtip devices are typically utilized to diminish or minimize the effects of tip vortices via controlling/suppressing tip vortex formation, like: winglets, sharklets and wingtip fences. In general, wings with winglets generate shorter and weaker tip vortex, compared to the wings without winglets.

By moving in the streamwise direction and getting farther from the wing tip, the vortex core diffuses in the lateral directions and circulation (strength of vortex) reduces under the effects of viscosity. 'Kevin's circulation theorem' describes the evolution of circulation in a flow field, here for an incompressible flow field. Mathematically 'Kevin circulation theorem' can be written as below:

$$\frac{D\Gamma}{Dt} = \underbrace{-\oint_C \frac{dp}{\rho}}_{barotropic\ term} - \underbrace{\oint_C \nu(\vec{\nabla} \times \vec{\omega}).d\vec{x}}_{diffusive/viscosity\ effects} \quad (2)$$

Where $\frac{D}{Dt}$ denotes a material temporal derivative operator. p and $\rho$are pressure and density, respectively. ν also represents kinematic viscosity. The first term on the RHS of Eq. (2) is negligible for most cases, except for barotropic flows. For our application here, i.e., flow over the cephalofoil of a hammerhead shark, the first term is omitted. The second term on the RHS of the equation indicates the effects of viscosity, as a monotonic decrease in circulation. In other words, the diffusive characteristics of viscosity tends to spread the vortex in the lateral direction towards its border and to decrease circulation quantity by getting farther and farther from the cephalofoil tip in the streamwise direction.

In the present research, to investigate evolution of the 'tip vortex strength', surface integral of the axial vorticity ω_x, as a major part of the circulation quantity, is considered over a rectangular window (Eq. (1)). The window is defined as $\Delta z \times \Delta y = [-0.3 \ldots 0.3] \times [-0.3 \ldots 0.3]$around the vortex core at each streamwise position behind the cephalofoil, i.e., x/b =0.25, 0.5, 0.75, 1.0, 1.5, 2.0, 3.0; where $b$is the cephalofoil span. In this regard, the vortex core at each vertical plane behind the cephalofoil is tracked by an in-house developed code using image processing techniques. The vortex core determines the centre of the abovementioned rectangular window.

Validation Test Case

Before switching to comparative CFD simulations of cephalofoil geometries, the adopted numerical strategy is first applied for simulations of fluid flow over a rectangular wing with unity aspect ratio at $Re \approx 1.5 \times 10^5$, as a validation test case (Taheri, 2021a). For low-aspect ratio wings, tip vortices are getting dominant over a larger portion of the wing; in this sense, lift coefficient slope decreases by lowering aspect ratio (Houghton et al., 2015). Figure 5 exhibits a very good agreement in variations of lift coefficient for the present numerical strategy in comparison to the experimental curve (Chen et al., 2012) and theoretical curve (Lowry & Polhamus, 1957). This validates the proposed numerical strategy to simulate flow over the cephalofoil of the hammer head shark, *S. lewini*.

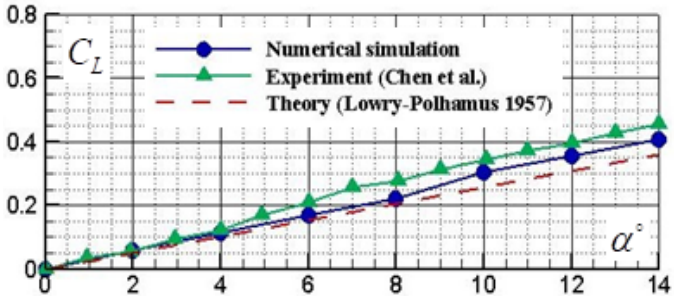

Figure 5. Lift coefficient versus AoA obtained from the adopted numerical strategy for a low-aspect ratio rectangular wing at $Re \approx 1.5 \times 10^5$

Results and Discussion

As mentioned, to study the hydrodynamic effects of cephalofoil tip eidonomy on tip vortex formation and evolution, a series of comparative turbulent flow simulations are performed. In the following sub-sections, obtained results are presented and discussed in details.

Bionic Winglet Behaviour at AoA

As discussed earlier, hammerhead sharks experience a wide range of AoAs and sideslip angles in their swimming envelope. Here, the effects of AoA variations on tip vortex evolution and characteristics are considered for the real and modified cephalofoil geometries (Figure 2). To detect the 'tip vortex' structure in the wake of a cephalofoil, different techniques can be adopted. In general, vortex detection schemes are classified into Eulerian and Lagrangian techniques; each with relative advantages and disadvantages. Basically, Eulerian techniques rely on the velocity gradient at a local point, such as λ_2-criterion. Figure 6 shows vortical structures developed over a cephalofoil for the real and modified geometries at $\alpha = 8^\circ$ and $\alpha = 16^\circ$, captured by $\lambda_2 = -1$. As one can see in the figure, the real cephalofoil (with tip bump) produces a shorter and weaker

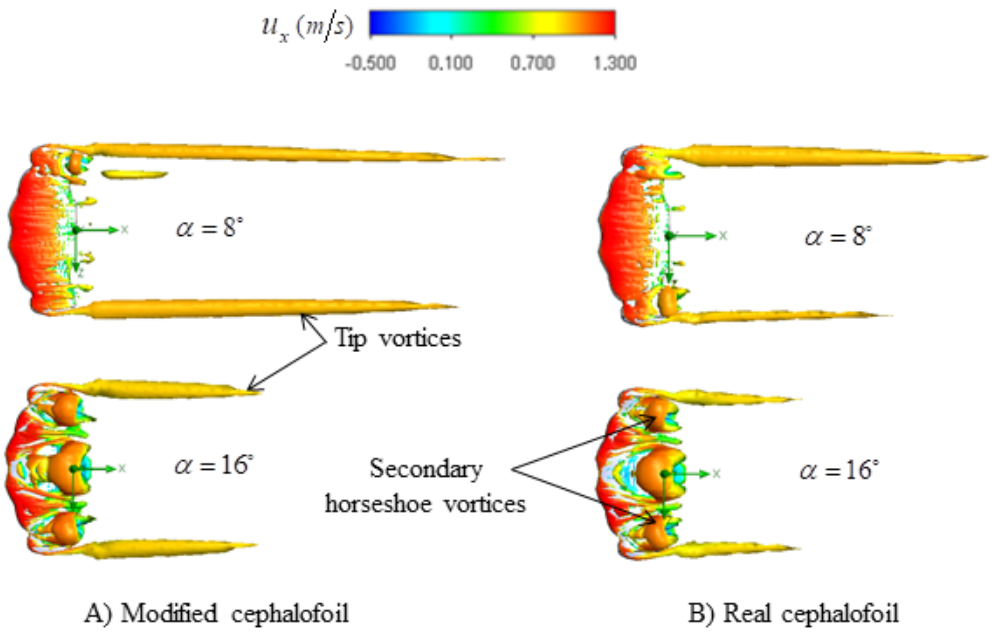

Figure 6. Tip vortices captured by λ_2-criterion ($\lambda_2 = -1$) for both real and modified cephalofoil geometries, coloured by axial velocity field

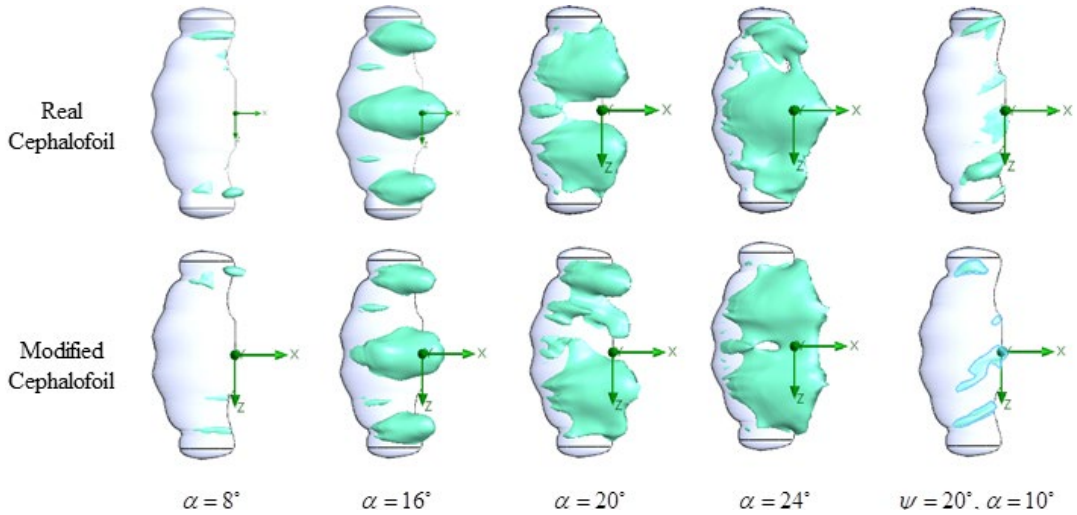

Figure 7. Flow separation zones over the real and modified geometries of the cephalofoil for different AoAs and a sideslip angle

tip vortex in its wake for both AoAs compared to the modified version. Secondary horseshoe vortices, bounded to the planform, are also generated and getting intensified by increasing AoA.

The evolution of flow separation zones (defined as, $u_x < 0$) at different AoAs and a sideslip angle is also visible in Figure 7. As one can see in the figure, for $\alpha < 16^\circ$, the topology of uncoherent separation zones is very similar for both cephalofoil geometries, although some minor differences exist. By increasing AoA, separation zones are getting larger and finally getting merged at $\alpha \approx 24^\circ$. For $\alpha > 16^\circ$, separation zone topology of the real cephalofoil deviates from the modified counterpart. At sideslip angle $\psi = 20^\circ$, separation zones are getting inclined, relative to the streamwise (x) direction. A different separation pattern forms for each version of the geometries, correlated to the wingtip eidonomy.

To visualize fluid flows passing over the cephalofoil, a tracer particle dynamic study has been performed here. In this regard, 10^3 spherical water particles with a diameter of 10^{-4} m are continuously released from the cephalofoil surface and are convected downstream by the bulk freestream flow. Ideal reflection is also applied for the fluid particle and wall interactions in the separation and recirculation zones, if any. Figure 8 indicates particle dynamics over the real cephalofoil. As one can see in the figure, primary tip vortices originating from the wing tip region and secondary vortices originating from the adjacent area of the wing tip are generated by special eidonomy of the cephalofoil. Later, more explanations about

the possible effects of these weak secondary vortices are provided. In addition, counter-rotating tip vortices are captured by iso-contours of axial vorticity, as $\omega_x = \pm 1$ 1/s (Figure 8).

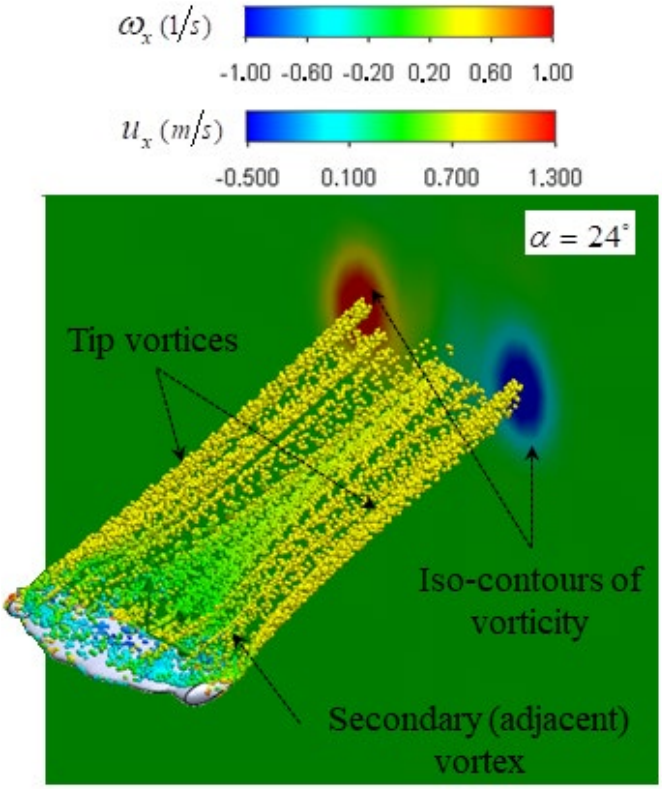

Figure 8. Tracer particle study result, superimposed with vorticity field at a downstream plane, i.e.,$x/b = 1.5$, behind the real cephalofoil at $\alpha = 24^\circ$

To further investigate characteristics of tip vortices of the cephalofoil, the evolution of axial vorticity fields at different downstream planes, perpendicular to the streamwise (x) direction, is considered here. As an example, Figure 9 exhibits axial vorticity fields behind the cephalofoil in the rectangular window $\Delta z \times \Delta y = [-0.3 \ldots 0.3] \times [-0.3 \ldots 0.3]$ around the tip vortex core. The planes are placed at x/b =0.25, 0.5, 1.0, 1.5, 2.0, and 3.0; where $b$is the cephalofoil span. As one can see in the figure, at x/b =0.25 an intensive tip vortex forms along with a weaker adjacent secondary vortex. It is also visible in the figure, by getting farther downstream at a larger distance from the cephalofoil trailing edge, viscosity acts more on the vorticity field and tends to reduce the vorticity gradient in the field, in accordance to 'Kevin's circulation theorem', Eq. (2). In this way, the maximum concentrated vorticity at x/b =0.25 (visible with dark color) are getting lower and lower towards x/b =3.0. Diffusion process, implemented by viscosity, spreads the tip vortex in the lateral directions through its boundary and increases the so-called 'vortex-affected area'. In other words, vortex tip cross-section grows under the effects of viscosity, although its strength (circulation) exhibits an overall decrease by getting farther from the cephalofoil tip according to 'Kevin's theorem'. It is worth mentioning that this decrease is not always monotonic in the case of cephalofoil geometry, in the following of this sub-section the reason will be presented and discussed in details. Another important observation visible in Figure 9 from x/b =0.25 to 3.0 is the 'merger event' of the tip vortex and the adjacent secondary vortex; this process potentially contributes to the variation of circulation, as discussed shortly in the following.

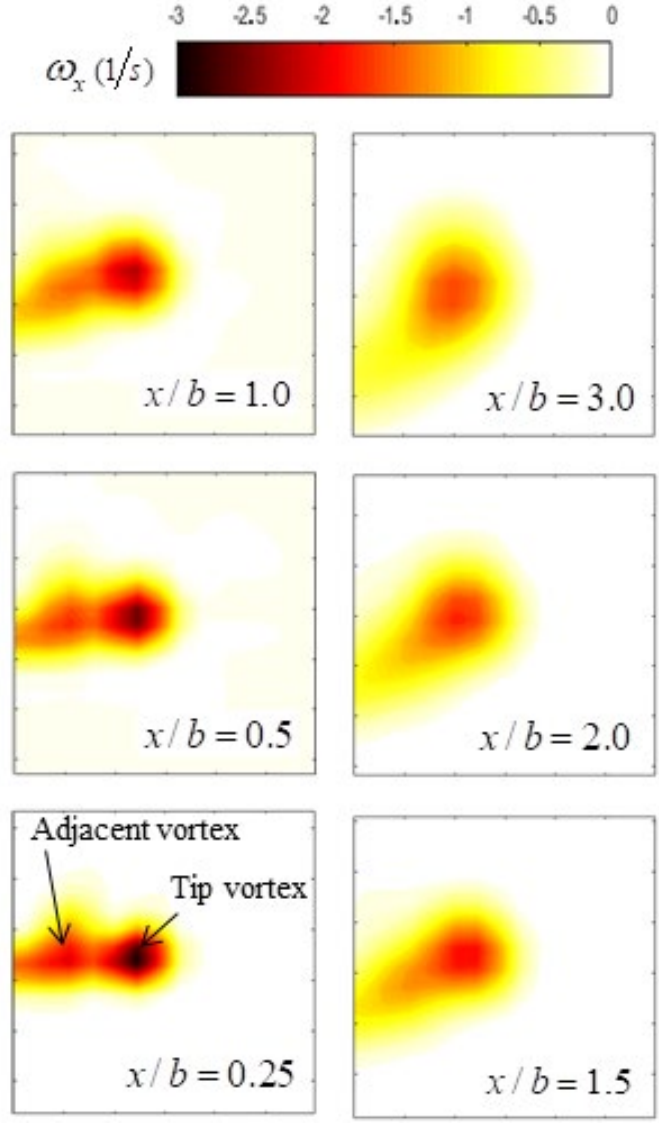

Figure 9. Evolution of tip vortex for the real cephalofoil in the streamwise direction at $\alpha = 8^\circ$, captured by axial vorticity field

As explained before, to quantify the possible effects of the cephalofoil tip geometry on the 'tip vortex' characteristics, variation of circulation (as a measure of vortex strength) in the streamwise (x) direction is considered here. As an instance, Figure 10 shows the variation of circulation (Γ) in the

streamwise direction at $\alpha = 16°$ and the maximum AoA in the present study, i.e., $\alpha = 28°$. As one can see in the figure, the circulation curve of the tip vortex for the real cephalofoil (with tip bump) is lower than one for the modified cephalofoil (without tip bump) at all streamwise positions for both AoAs. By increasing AoA, the effect is getting more pronounced. The curves demonstrate that cephalofoil bump in the eye bulb region of a hammerhead shark behaves as a winglet and produces a weaker tip vortex (with lower circulation value) compared to the version without the tip bump.

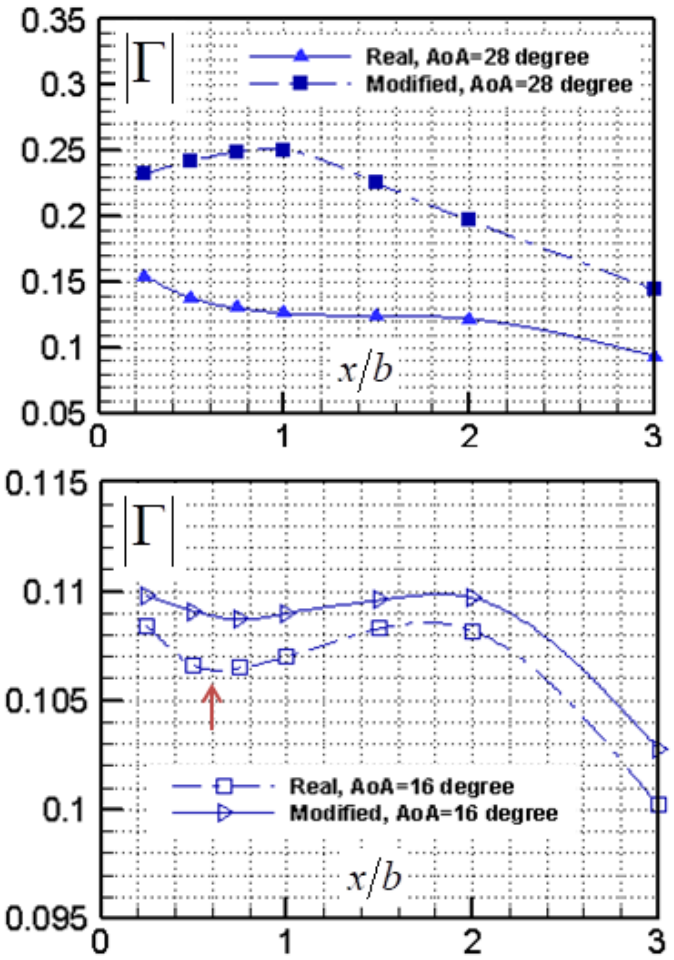

Figure 10. Variation of circulation for the real and modified cephalofoil geometries of the hammerhead shark in the streamwise direction at $\alpha = 16°$ (bottom) and $\alpha = 28°$ (top)

It is also important to notice that for an individual single vortex 'Kevin's circulation theorem' suggests that the circulation of tip vortex in streamwise direction monotonically decreases by viscosity, such as circulation curve obtained for the real cephalofoil geometry at $\alpha = 28°$ in Figure 10. On the other hand, as shown in the figure for $\alpha = 16°$, there exists an initial decrease in the circulation curve up to about $x/b = 0.6$. In the interval, $0.6 < x/b < 2.0$, circulation increases and for $x/b > 2.0$ circulation decreases again in the streamwise direction for both versions of the cephalofoil geometry. The physics responsible for the abovementioned behaviour is the 'merger phenomenon' of the tip vortex and the secondary (adjacent) vortex, as mentioned earlier (Figure 9). In fact, the monotonic decrease for the circulation in the interval $0 < x/b < 0.6$, as predicted by 'kevin's theorem' is valid for a single tip vortex. At $x/b = 0.6$ (marked by a vertical red arrow in Figure 10), tip vortex and the secondary (adjacent vortex) start to interact over the interval $0.6 < x/b < 2.0$ in a nonlinear fashion and are completely merged at around $x/b = 2.0$ and forms a stronger single vortex with higher level of circulation (strength). This process explains the observed nonlinear increase of the circulation over $0.6 < x/b < 2.0$. For $x/b > 2.0$, circulation of the single resultant tip vortex (resultant of the merger phenomenon) decreases again under the viscosity effects in a nonlinear fashion as predicted by 'Kevin's circulation theorem'. Figure 11 shows similar trends for variations of circulation of tip vortices in the streamwise direction at other simulation AoAs for the real and modified cephalofoil geometries. It is also visible in the figure that the strength of cephalofoil tip vortices gets augmented by increasing AoA.

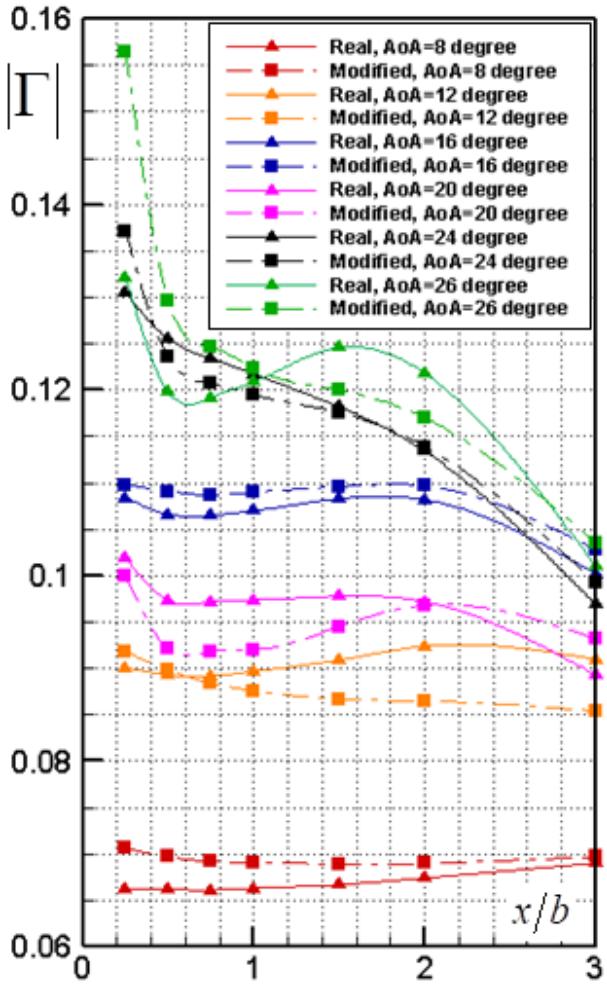

Figure 11. Variations of circulation (Γ) in the streamwise direction (x/b) for the real and modified cephalofoil geometries at all simulation AoAs

Bionic Winglet Behaviour at Sideslip Angle

As mentioned before, hammerhead sharks are agile swimmers, facing to a wide range of AoAs, sideslip and roll angles in their manoeuvres. Here in the final section, turbulent flows over both geometric versions of the cephalofoil are simulated at a sideslip angle $\psi = 20^\circ$ along with $\alpha = 10^\circ$. Figure 12 depicts vortical structure captured by $\lambda_2 = -1$ criterion.

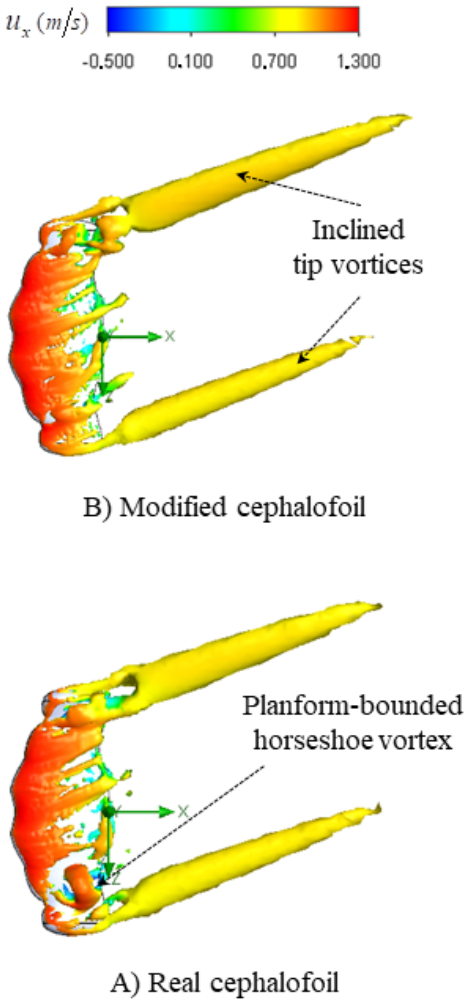

Figure 12. Vortical structure formation over the real and modified versions of the cephalofoil at sideslip angle ($\psi = 20^\circ$ and $\alpha = 10^\circ$)

As one can see in Figure 12, tip vortices are deflected and getting inclined due to the sideslip blowing angle $\psi = 20^\circ$. A planform-bounded horseshoe vortex is also generated near the cephalofoil tip for the real version of the geometry, which is not present for the modified version of the geometry. Figure 13 depicts the variation of circulation in the streamwise direction for the flow simulation at the sideslip angle $\psi = 20^\circ$. As it is visible in the figure, the circulation quantity decreases in the streamwise direction in agreement with Kevin's theorem. The real geometry of the cephalofoil behaves slightly better than the modified version at the sideslip angle, although the difference in circulation vanishes by getting farther downstream in the streamwise (x) direction.

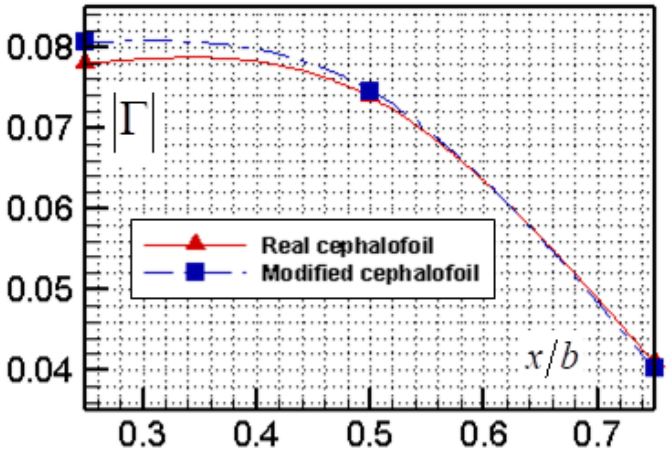

Figure 13. Variations of circulation behind the cephalofoil for both geometric versions in the streamwise direction at $\psi = 20^\circ$ and $\alpha = 10^\circ$

Conclusion

In the present research, it was shown that the special eidonomy of the cephalofoil tip of a scalloped hammerhead shark, *S. lewini*, exhibits winglet-type behaviour. It produces weaker and shorter tip vortices, similar to the functionality of winglets for airplanes. In fact, by special hammerhead-shape of the head and the corresponding position of its eyes, *S. lewini* takes advantages of wider ocular vision, olfactory and electro-sensory capabilities. In addition, bump at the cephalofoil tip (basically formed by the eye bulb) brings a favourable hydrodynamic characteristic for the swimming hammerhead shark by reducing the strength of tip vortices over a wide range of AoA and sideslip angles. It was also shown that the observed local increase in the circulation of the tip vortices in the streamwise direction corresponds to a nonlinear merger of the cephalofoil tip vortex and another vortical structure, originating from an adjacent region of the cephalofoil tip. Following a nonlinear transition period (after the merger event), a monotonic decrease in the circulation is restored, as expected by 'Kevin's circulation theorem' under the effects of viscosity. As turbulent flow simulations suggest, winglet effects of the cephalofoil tip decrease at sideslip angles.

Acknowledgements

The author would like to sincerely acknowledge every single effort done by institutes, organizations and individuals for the protection of 'hammerhead sharks' worldwide.

Compliance With Ethical Standards

Conflict of Interest

The author declares that there is no conflict of interest.

Ethical Approval

For this type of study, formal consent is not required.

References

Bang, K., Kim, J., Lee, S. I., & Choi, H. (2016). Hydrodynamic role of longitudinal dorsal ridges in a leatherback turtle swimming. *Scientific Reports*, *6*, 34283. https://doi.org/10.1038/srep34283

Battista, N. A. (2020). Swimming through parameter subspaces of a simple anguilliform swimmer. *Integrative and Comparative Biology*, *60*(5), 1221–1235, https://doi.org/10.1093/icb/icaa130

Borazjani, I. (2008). Numerical simulations of fluid-structure interaction problems in biological flows. [Ph.D. Thesis. University of Minnesota].

Chen, J. H., Li, S. S., & Nguyen, V. T. (2012). The effect of leading edge protuberances on the performance of small aspect ratio foils. *Proceedings of the 15th International Symposium on Flow Visualization*, Belarus, pp. 1-16.

Copmpagno, L., Dando, M., & Fowler, S. (2005). *Sharks of the world* (1st ed.). Princeton University Press.

Domel, A. G., Saadat, M., Weaver, J. C., Haj-Hariri, H., Bertoldi, K., & Lauder, G. V. (2018). Shark skin-inspired designs that improve aerodynamic performance. *Journal of Royal Society Interface*, *15*, 1-9. https://doi.org/10.1098/rsif.2017.0828

Fish, F. E., Schreiber, C. M., Moored, K. W., Liu, G., Dong, H., & Bart-Smith, H. (2016). Hydrodynamic performance of aquatic flapping: efficiency of underwater flight in the manta. *Aerospace Journal*, *3*(20), 1-24. https://doi.org/10.3390/aerospace3030020

Gaylord, M. K., Blades, E. L., & Parsons, G. R. (2020). A hydrodynamics assessment of the hammerhead shark cephalofoil. *Scientific Reports, 10*, 14495. https://doi.org/10.1038/s41598-020-71472-2

Houghton, E. L., Carpenter, P. W., Collicott, S. H., & Valentine, D. T. (2015). *Aerodynamics for Engineering Students* (Seventh Edition). Elsevier Ltd. Publication.

Kajiura, S. M., Forni, J. B., & Summers, A. P. (2003). Maneuvering in juvenile carcharhinid and sphyrnid sharks: the role of the hammerhead shark cephalofoil. *Zoology, 106*, 19–28. https://doi.org/10.1078/0944-2006-00086

Kajiura, S. M., Forni, J. B., & Summers, A. P. (2005). Olfactory morphology of carcharhinid and sphyrnid sharks: Does the cephalofoil confer a sensory advantage?. *Journal of Morphology*, *264*, 253-263. https://doi.org/10.1002/jmor.10208

Ketchum, J. T., Hearn, A., Klimley, A. P., Espinoza, E., Peñaherrera, C., & Largier, J. L. (2014). Seasonal changes in movements and habitat preferences of the scalloped hammerhead shark (*Sphyrna lewini*) while refuging near an oceanic island. *Marine Biology*, *161*, 755–767. https://doi.org/10.1007/s00227-013-2375-5

Kuznar, Sh. (2017). Morphological variation in olfactory, optic, and electrosensory structure of juvenile scalloped hammerhead sharks (*Sphyrna lewini*) [Master Thesis. Purdue University].

Lam, C. K. G., & Bremhorst, K. A. (1981). A modified form of the $k-\varepsilon$ model for predicting wall turbulence. *Journal of Fluid Engineering*, *103*, 456–460. https://doi.org/10.1115/1.3240815

Lowry, J. G., & Polhamus, E. C. (1957). *A method for predicting lift increments due to flap deflection at low angles of attack in incompressible flow*. Report, University of North Texas Libraries.

McComb, D. M., Tricas, T. C., & Kajiura, S. M. (2009). Enhanced visual fields in hammerhead sharks. *Journal of Experimental Biology, 212,* 4010-4018. https://doi.org/10.1242/jeb.032615

Miklosovic, D. S., Murray, M. M., Howle, L. E., & Fish, F. E. (2004). Leading-edge tubercles delay stall on humpback whale (*Megaptera novaeangliae*) flippers. *Physics of Fluids*, *16*, 39-42. https://doi.org/10.1063/1.1688341

Miles, J. G., & Battista, N. A. (2019). Naut your everyday jellyfish model: exploring how tentacles and oral arms impact locomotion. *Fluids Journal*, *4*(169), 1-43. https://doi.org/10.3390/fluids4030169

Payne, N. L., Iosilevskii, G., Barnett, A., Fischer, C., Graham, R. T., Gleiss, A. C., & Watanabe, Y. Y. (2016). Great hammerhead sharks swim on their side to reduce transports costs. *Nature Communication*, *7*(12289), 1-5. https://doi.org/10.1038/ncomms12289

Royer, M., Maloney, K., Meyer, C., Cardona, E., Payne, N., Whittingham, K., Silva, G., Blandino, C., & Holland, K. (2020). Scalloped hammerhead sharks swim on their side with diel shifts in roll magnitude and periodicity. *Animal Biotelemetry*, *8*, 11. https://doi.org/10.1186/s40317-020-00196-x

Sobachkin, A., & Dumnov, G. (2013). Numerical basis of CAD-Embedded CFD. *Proceedings of the NAFEMS World Congress*, Austria, pp. 1-19.

Taheri, A. (2018a). Lagrangian coherent structure analysis of jellyfish swimming using immersed boundary FSI simulations. *Journal of Mechanical and Civil Engineering*, *15*(1), 69-74. https://doi.org/10.9790/1684-1501046974

Taheri, A. (2018b). A meta-model for tubercle design of wing planforms inspired by humpback whale flippers. *International Journal of Aerospace and Mechanical Engineering*, *12*(3), 315-328. https://doi.org/10.5281/zendoo.1317268

Taheri, A. (2018c). On the hydrodynamic effects of humpback whale's ventral pleats. *American Journal of Fluid Dynamics*, *8*(2), 47-62. https://doi.org/10.5923/j.ajfd.20180802.02

Taheri, A. (2020). Hydrodynamic impacts of prominent longitudinal ridges on the 'whale shark' swimming. *Research in Zoology*, *10*(1), 18-30. https://doi.org/10.5923/j.zoology.20201001.03

Taheri, A. (2021a). *Fluid dynamics and bio-propulsion of animal swimming in nature: Bionics* (1st ed.). Arshadan Publication.

Taheri, A. (2021b). Lagrangian flow skeletons captured in the wake of a swimming nematode *C. elegans* using an immersed boundary fluid-structure interaction approach. *International Journal of Bioengineering and Life Sciences, 15*(7), 71-78.

Taheri, A. (2021c). Hydrodynamic analysis of bionic chimerical wing planforms inspired by manta ray eidonomy. *Indonesian Journal of Engineering and Science, 2*(3), 11-28. https://doi.org/10.51630/ijes.v2i3.25